Exploration of alternative mask for 0.33NA extreme ultraviolet single patterning at pitch 28-nm metal design

Dongbo Xu,* Werner Gillijns, Ling Ee Tan, Vicky Philipsen, and Ryoung-Han Kim
imec, Leuven, Belgium

Abstract. Extending 0.33NA extreme ultraviolet (EUV) single patterning to pitch 28 nm will enable significantly shorter process flow for N2 node and cost-efficiency of metal layers patterning. At the same time, EUV single patterning becomes very challenging in terms of stochastic defectivity and process window. To enable EUV single patterning at pitch 28 nm with good process window and patterning fidelity (low defectivity and line edge roughness), three mask candidates are considered: a standard binary Ta-based absorber mask, a high extinction (high-k) absorber mask, and a low-n attenuated phase-shift mask (attPSM). The patterning performance of these three mask candidates is compared by means of source mask optimization. The patterning performance of the candidate masks is assessed using an imec N3 (foundry N2 equivalent) random logic M1 layout. The impact of mask tonality (bright field versus dark field) and insertion of sub-resolution assist features (SRAFs) on pattern fidelity and process window is evaluated. Considering all the aspects, simulations indicate that the low-n attPSM has the best patterning performance both for dark-field mask with SRAFs and bright-field mask without SRAFs.
 [DOI: 10.1117/1.JMM.21.2.024401]

Keywords: extreme ultraviolet single patterning; mask absorber; source mask optimization; logic; pitch 28 nm.

Paper 21089G received Nov. 3, 2021; accepted for publication Mar. 14, 2022; published online Apr. 7, 2022.

1 Introduction

To further reduce the manufacturing cost and process complexity at advanced technology nodes, a number of layers using extreme ultraviolet lithography (EUVL) patterning will be increased significantly.[1] Therefore, extending 0.33NA EUV single patterning to pitch 28 nm is very meaningful for high volume manufacturing, which is under development and evaluation at imec.[2–6] However, EUV single patterning at pitch 28 nm becomes very challenging in terms of stochastic defectivity and process window. The increased importance of stochastic effects at pitch 28 nm demands high contrast lithographic images. In EUVL, mask three-dimensional (M3D) effects have a significant impact on lithographic imaging, which can introduce telecentricity errors (TCEs), best focus shift through pitch and through slit printability issues at wafer level.[7–10] Specifically, the M3D phase differences lead to image contrast loss due to image fading.[5] To mitigate the M3D effects, one approach is to employ alternative mask stacks, high extinction (high-k) absorber masks, and low-n attenuated phase-shift masks (attPSMs) have been investigated and evaluated in the past.[9,11–19] Another approach is adapting the illumination source shape to mitigate image fading caused image contrast loss due to the M3D effects.[4,5,10,20,21]

In this paper, three mask candidates are studied by using a commercial source mask optimization (SMO) tool, which can help us to optimize the compromised overall process window (OPW) of a certain design, and delivers the best illumination source. The standard binary Ta-based absorber mask is used as the reference, two alternative mask candidates are included: a high-k absorber mask and a low-n attPSM.[17] The M1 layer of an imec N3 (foundry N2 equivalent) random logic design is used to assess the patterning performance for these three mask candidates, and various metrics are employed to quantify the patterning quality. Both the impact

*Address all correspondence to Dongbo Xu, dongbo.xu@imec.be

1932-5150/2022/$28.00

of mask tonality (bright field versus dark field) and insertion of sub-resolution assist features (SRAFs) are investigated. To avoid tone inversion and keep low process complexity and cost, a dark-field EUV mask is employed with a positive tone development (PTD) process and a bright-field EUV mask is combined with a negative tone development (NTD) process.

This paper is organized as follows: Section 2 introduces the SMO strategy, and the results of SMO for pitch 28-nm line/space grating are discussed. Section 3 investigates the patterning performance of the M1 layer of an imec N3 random logic design at pitch 28 nm. The impact of mask tonality and insertion of SRAFs on the OPW and patterning quality is evaluated. Section 4 will provide the conclusion.

2 Source Mask Optimization Strategy

The simulations of pitch 28-nm EUV single patterning use case are performed assuming an ASML 0.33NA NXE:3400 EUV scanner.[22] Three mask candidates are considered, a standard binary Ta-based absorber mask used as the reference, a high-k absorber mask, and a low-n attPSM. The binary mask has a 60-nm-thick Ta-based absorber. The absorber thickness of the high-k mask and the low-n attPSM are optimized in the paper of Erdmann et al.,[17] to obtain the best normalized image log-slope (NILS). The details of multilayer stack information are described in the paper of Makhotkin et al.[23] A blur of 2 nm is used in the aerial image simulation to mimic the resist blur of the assumed patterning process. The ASML Tachyon SMO-MO flow[24,25] is used to evaluate the impact of mask tonality and insertion of SRAFs on patterning performance by optimizing model threshold, best focus, and mask correction.

2.1 *Input Target*

Figure 1 shows the design clip that is used for the simulation study in the paper, which is 1 μm^2 imec N3 random logic design. Analysis of the design helps us to identify yield limiters.

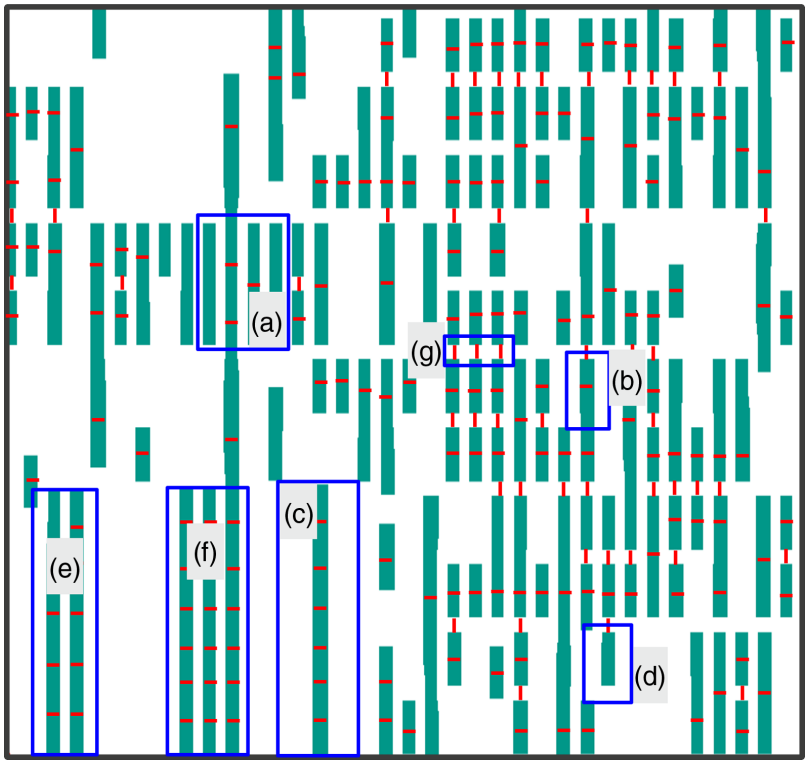

Fig. 1 imec N3 random logic design clip with design retargeting: (a) dense line/space, minimum pitch is 28 nm, minimum trench CD is 14 nm, (b) and (d) semi-isolated features, (c) isolated feature, (e) two-bar, (f) three-bar, (g) T2T, CD is 20 nm. Semi-isolated and isolated features target CD are between 14 and 18 nm. The red cutlines are used in Sec. 3.1 for OPW evaluation.

As shown in Fig. 1, we deal with various configurations of line/space and tip-to-tip (T2T) patterns: (a) dense, (b) semi-isolated with symmetric context, (c) isolated, and (d) semi-isolated with asymmetric context. The minimum pitch and minimum trench critical dimension (CD) of 1D features is 28 and 14 nm, respectively. Design retargeting is applied to the design to make patterning more robust, as well to compensate for litho-etch bias from dense to isolated features. Therefore, the trench CDs through pitch are varying from 14 to 18 nm. The minimum T2T CD is 20 nm. The red cutlines are used for OPW evaluation in Sec. 3.1.

2.2 *SMO Job Setup*

The default EUV SMO template for NXE:3400 in the SMO tool is used. The pupil illumination efficiency is set to 100% and a uniform flare level of 2% is considered.[26] To guarantee the required image quality at de-dose, de-focus conditions, four combinations of $\pm 10\%$ delta dose with ± 40 nm delta focus are used in the optimization. The SMO was first run on a vertical dense pitch 28 nm 1:1 line/space grating as the input target, this choice is motivated by several aspects:

1. The imec N3 random logic design clip shown in Fig. 1 contains mainly vertical metal trenches, the minimum pitch and minimum trench CD are 28 and 14 nm, respectively.
2. Previous studies have shown that stochastic printing failures are critical in EUVL patterning at tight pitches.[27–29] Higher NILS is important for EUVL patterning to have good control of the stochastic failures; only using pitch 28 nm 1:1 line/space grating as the input target guarantees high NILS on these trenches.
3. Patterning vertical trenches through pitch is currently our first priority. Therefore, we give a lower priority on T2T.
4. The area covered by the absorber is the same as the open mirror area for pitch 28 nm 1:1 line/space grating; therefore, the obtained sources can be used both for bright field and dark-field masks MO evaluation.

2.3 *Source Optimization for Pitch 28-nm Line/Space Grating*

Figure 2 shows the optimized sources with respect to these three mask candidates when using vertical pitch 28 nm 1:1 line/space grating as the input target. All of them are dipole sources with a minor difference after source rendering. Figure 3 shows the comparison of exposure latitude (EL) and NILS of pitch 28-nm line/space grating with respect to these three mask candidates. The high-k absorber mask and the low-n attPSM are able to increase both EL and NILS through focus for pitch 28-nm line/space grating with respect to the reference binary mask. However, the imec N3 random logic design (Fig. 1) contains not only pitch 28-nm line/space grating but also semi-isolated and isolated features, two-bars, three-bars, and short metals at the random patterns region. The optimized sources will be used in Sec. 3 to evaluate the lithographic performance of these three mask candidates for patterning this logic design.

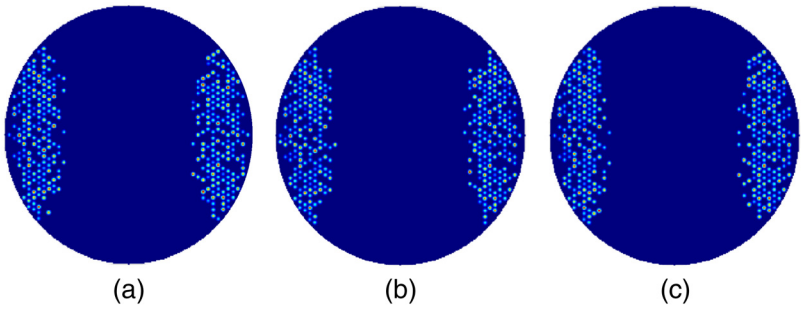

Fig. 2 Using vertical pitch 28-nm line/space grating as the input target, SMO optimized sources with respect to these three mask candidates: (a) source for the reference binary mask, (b) source for the high-k absorber mask, and (c) source for the low-n attPSM.

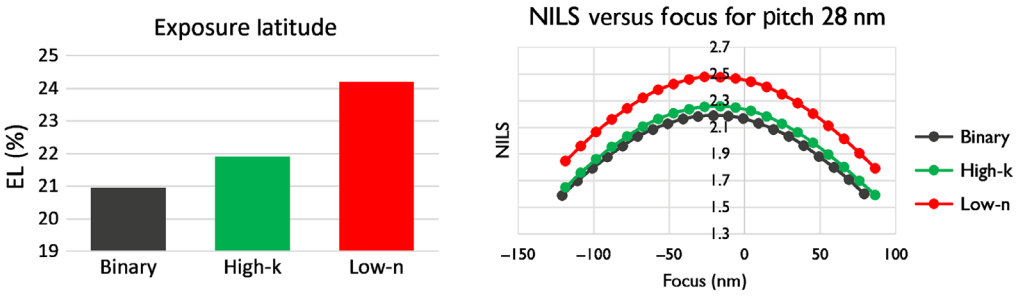

Fig. 3 EL and NILS through focus comparison for these three mask candidates. SMO input clip is vertical pitch 28 nm 1:1 line/space grating. The corresponding illumination sources are shown in Fig. 2.

3 Benefit of Alternative Mask Candidates on Patterning Pitch 28-nm Random Logic Design

This section is focusing on using MO to study the impact of these three mask candidates on the OPW and patterning quality of a random logic pitch 28-nm design (as shown in Fig. 1) using EUV single patterning. The used sources are optimized in Sec. 2.3. In MO jobs, the mask rule check (MRC) constraints are set to 8 nm at wafer-level scale (1×) for T2T CD, space, and line CD; the SRAF CD is set to 6 nm (1×). Several metrics are used in our study to evaluate the benefit of these three mask candidates:

1. The CD-based OPW is used to characterize the process capability. The trench CD and T2T CD variations within ±10% and ±20%, respectively, are used in the study to define the process window; larger OPW indicates better process window tolerance.
2. The NILS is inversely proportional to stochastic effects.[30] Higher NILS is important for EUVL to have good control of the stochastic variability.
3. The best focus shifts of the design features limit the OPW.
4. The mask error enhancement factor (MEEF) plays an important role in the design for manufacturing and resolution enhancement technology flow at advanced technology nodes. The MEEF of an ideal linear imaging system is one, which means that the wafer CD errors correspond exactly to the mask CD errors.
5. TCEs result in pattern placement errors (PPE) through a focus on the wafer.

In the paper, we are focusing on the vertical design, and our first priority is patterning line/space patterns through a pitch. Our goal is to study the patterning performance when using these three mask candidates by evaluating the selected metrics.

3.1 *Overall Process Window*

3.1.1 *Dark-field mask*

Figure 4 shows the OPWs of dark-field masks with and without insertion of SRAFs at the center slit for these three mask candidates. The OPW is calculated on the cutlines shown in red in Fig. 1. The left column presents the OPWs of MO without SRAFs, and the right column displays the OPWs of MO with SRAFs. Comparing the results of the reference binary mask, the MO with SRAFs gives us slightly better OPW, increased EL, and depth of focus (DoF) over the MO without SRAFs.

Comparing the results of the alternative mask candidates to the reference binary mask, the OPW of the high-k absorber mask has increased overall EL by ∼20% for both MO with and without SRAFs. The low-n attPSM MO without SRAFs does not have an OPW due to the large best focus shifts among different features. The study of van Lare et al.[31] indicates this is due to M3D phase offsets among diffraction orders of different features. The low-n attPSM MO with SRAFs is able to suppress these best focus shifts, which increases the overall EL by ∼10% with

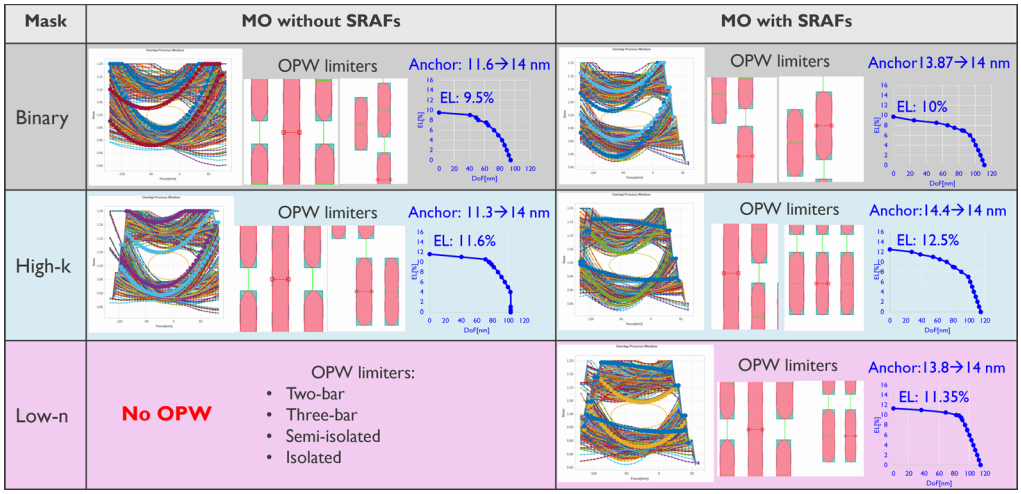

Fig. 4 OPWs (±10% CD tolerance on trenches and ±20% CD tolerance on T2Ts) of the three dark-field mask candidates with and without SRAFs insertion at the center slit. The OPW is calculated using cutlines shown in Fig. 1. The thick lines in the OPW correspond to the red cutlines on the clips to highlight the OPW limiters.

respect to the reference binary mask. By insertion of SRAFs, the high-k absorber mask and the low-n attPSM gain more overall EL than the reference binary mask. Figure 5 shows the SRAF positions and sizes for two-bar, three-bar, and Iso features, which indicates that the high-k absorber mask needs slightly larger SRAFs, whereas the low-n attPSM requires slightly smaller SRAFs with respect to the reference binary mask. The OPW limiters for each mask candidate are also shown in Fig. 4:

1. The OPWs of the standard binary mask and the high-k absorber mask are limited by the best focus shift between isolated features and two-bar short metals;
2. No OPW was obtained for the low-n attPSM MO without SRAFs, due to the large best focus shifts among dense line/space, two-bar, three-bar, semi-isolated, and isolated features.
3. The low-n attPSM with SRAFs reduces the best focus shifts among different types of features, the limiters are the isolated trench between T2Ts and semi-isolated short metals.

3.1.2 *Bright-field mask*

Figure 6 shows the OPWs of bright-field masks with and without insertion of SRAFs at the center slit for these three mask candidates. The left column contains the OPWs of MO without SRAFs, and the right column presents the OPWs of MO with SRAFs. The OPW of binary mask indicates that MO with SRAFs is able to increase both overall EL and DoF with respect to MO without SRAFs.

Compared with the reference binary mask, for the MO without SRAFs, the OPW of high-k absorber mask has similar overall EL but with ∼10% increased overall DoF; and the OPW of

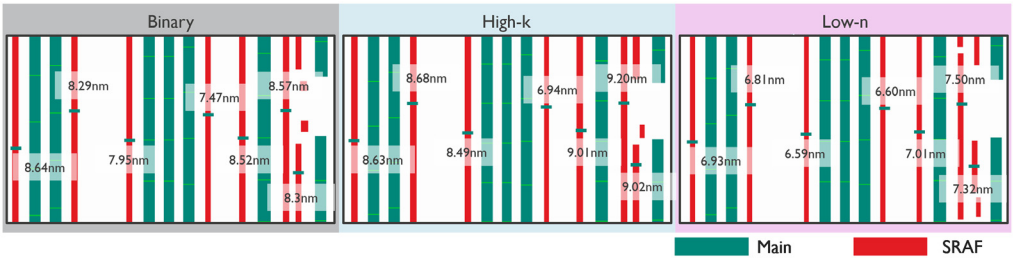

Fig. 5 SRAF size comparison for these three dark-field masks.

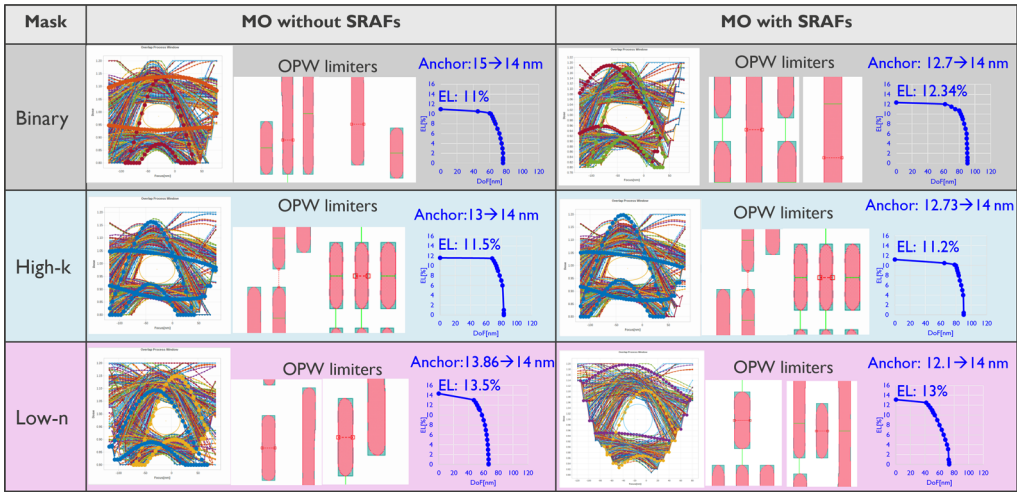

Fig. 6 OPW (±10% CD tolerance on trenches and ±20% CD tolerance on T2Ts) table of the bright-field mask candidates with and without SRAFs insertion at the center slit. The OPW is calculated using cutlines shown in Fig. 1. The thick lines in the OPW correspond to the red cutlines on the clips to highlight the OPW limiters.

low-n attPSM has a similar overall DoF but with ∼20% increased overall EL. However, comparing OPWs between the left and right column, the high-k absorber mask, and the low-n attPSM MO do not gain in OPW when applying SRAFs. The optimized mask layout of MO with SRAFs indicates only a few small SRAFs are randomly placed, which means it is difficult to insert 6 nm or larger SRAFs to the mask layout during MO to further improve the OPW without inducing SRAF printability. A smaller MRC value is needed for a bright-field mask, which is too aggressive for current mask technology. The OPW limiters for each mask type are also shown in Fig. 6:

1. The OPW of the reference binary mask is limited by the best focus shift between three-bar and isolated features.
2. The OPW of high-k absorber mask is limited by the best focus shift between three-bar short metals and more isolated T2Ts.
3. The OPW of low-n attPSM is limited by the best focus shift between semi-isolated short metals and isolated features.

In general, the OPW results in Figs. 4 and 6 show that 0.33NA EUV single patterning at pitch 28 nm: if the process is limited to a PTD process, a dark-field mask with the insertion of SRAFs delivers the best OPW for these three mask candidates; otherwise, a bright-field mask without SRAFs using an NTD process delivers the best OPW. The MO is optimized through a slit, and similar results are observed at the edge slit. Therefore, in the following sections, we will focus on the dark-field mask with insertion of SRAFs and the bright-field mask without insertion of SRAFs for these three mask candidates, to compare in detail by using relevant imaging metrics.

3.2 *Impact on NILS*

3.2.1 *NILS of trenches at best focus*

Figure 7 shows the NILS map of all the trenches across the design clip and the corresponding histogram distribution at nominal conditions. The Gaussian function is used to fit the NILS histogram distribution, and the fitting mean and standard deviation (σ) are displayed below each plot. The NILS map is obtained by densely placing the cutlines on the trenches shown in Fig. 1. The histogram distribution is obtained by binning cutlines per density via design rule check: the dense bin covers the trenches with 28-nm pitch to the other trenches on both sides, whereas the semi-isolated bin refers to the trenches with 28-nm pitch only on one side and the isolated bin refers to the trenches with >28-nm pitch on both sides to the other trenches. The top two rows in

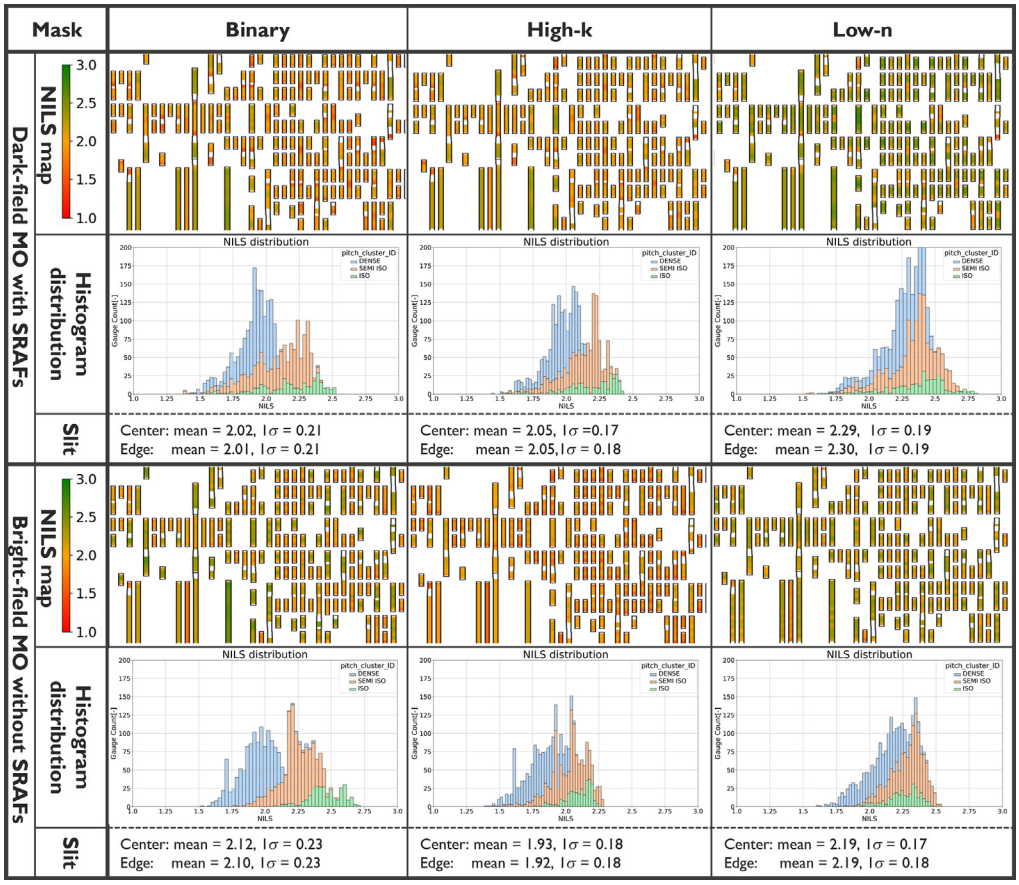

Fig. 7 NILS map of all the trenches across the design clip and the corresponding histogram distribution at the nominal condition for these three mask candidates. The Gaussian function is used to fit the NILS histogram distribution, the fitting mean, and standard deviation (σ) are displayed below each plot.

Fig. 7 are the NILS maps and histogram distributions of dark-field MO with SRAFs, and the bottom two rows are the NILS maps and histogram distributions of bright-field MO without SRAFs. The Gaussian function is used to fit the NILS histogram distribution both for center slit and edge slit, both high-k absorber mask and low-n attPSM have a similar NILS variation range than the reference binary mask:

1. The high-k absorber dark-field mask with SRAFs has a very similar NILS distribution with respect to the reference binary dark-field mask. The NILS of the high-k absorber bright-field mask without SRAFs is degraded by ∼10% with respect to the reference binary bright-field mask.
2. The low-n attPSM is able to improve the NILS by ∼15% for dark-field MO with SRAFs and ∼5% for bright-field MO without SRAFs. More specifically, the low-n attPSM significantly increases the NILS distribution of dense and semi-isolated line/space for these two cases; NILS of isolated features gains less improvement.

3.2.2 *NILS of trenches at ±20 nm defocus*

To evaluate the image quality through focus, Fig. 8 shows the NILS variation through focus (±20 nm) at center slit. Gaussian fittings of NILS distribution at each position are shown at the bottom of each plot. The top row shows the NILS distributions of dark-field MO with SRAFs and the bottom row shows the NILS distributions of bright-field MO without SRAFs. The alternative plots of the NILS distribution provide further insights. First, let us compare the data in the top row. With respect to the best focus, the NILS distributions of the high-k absorber mask have a slight NILS degradation at positive defocus (especially for the isolated features),

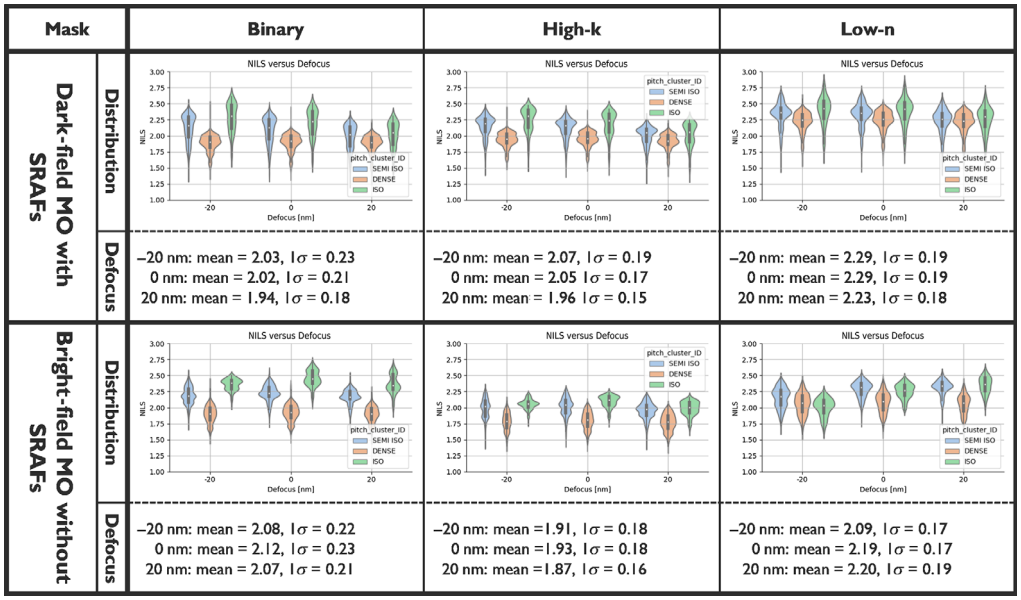

Fig. 8 NILS histogram distributions of trenches across the design clip at best focus and ±20 nm defocus for these three mask candidates at the center slit. The Gaussian function is used to fit the NILS histogram distribution, below each plot lists the mean and standard deviation (σ) through focus.

whereas NILS distribution is unchanged at negative defocus, this behavior is very similar to the reference binary dark-field mask. Low-n attPSM has unchanged NILS distribution through focus. Now, let us look at the data in the bottom row: NILS distributions of the high-k absorber mask and the binary mask do not change much through focus, whereas the low-n attPSM leads to slight NILS degradation at negative defocus (especially for the isolated features).

3.2.3 *NILS of T2Ts at best focus*

Figure 9 displays the NILS histogram distributions on T2Ts at the best focus for these three mask candidates. The top row shows the results of dark-field MO with SRAFs, and the bottom row

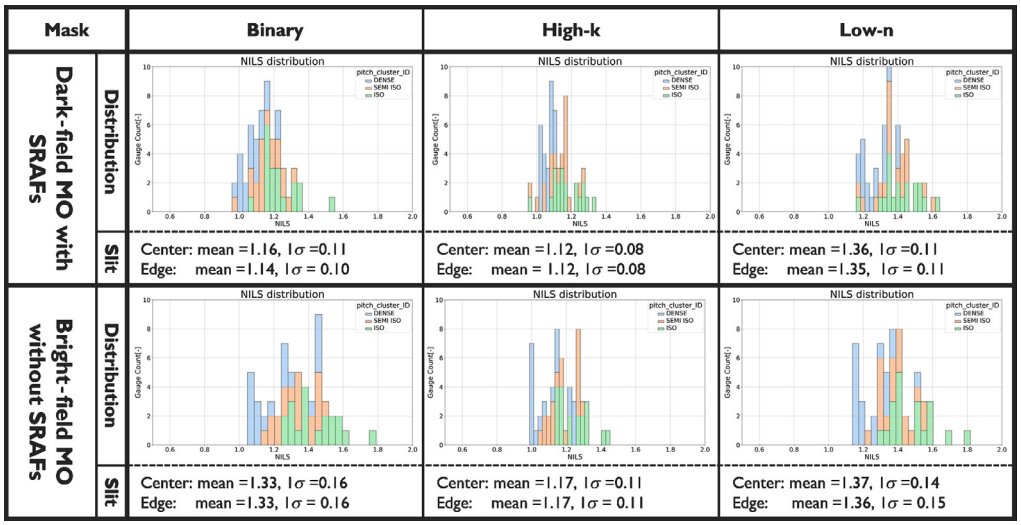

Fig. 9 NILS histogram distribution of T2Ts across the design clip at the nominal condition for these three mask candidates. Distribution is fitted by a Gaussian function and the fitting mean and standard deviation (σ) are displayed below each plot.

contains the results of bright-field MO without SRAFs. The low-n attPSM provides slightly better NILS for both cases, whereas the high-k absorber mask delivers slightly worse NILS of T2Ts with respect to the reference binary mask for both cases.

Since MO is able to optimize the mask through the slit to mitigate the M3D effect, a very similar NILS distribution was observed at the edge slit as well. The comparison of NILS distributions among these three mask candidates indicates that the low-n attPSM is able to provide the best NILS for patterning pitch 28-nm vertical design, which implies a good control of stochastic variability.[30]

3.3 *Impact on Best Focus Shift*

3.3.1 *Best focus shift of trenches*

Figure 10 presents the best focus shifts of various features on the design clip for these three mask candidates. The dark-field MO with SRAFs of the high-k absorber mask and the low-n attPSM have smaller best focus shifts through the pitch with respect to bright-field MO without SRAFs. SRAFs have the capability to correct the Bossung tilts and to mitigate the associated best focus shift.[32] For the bright-field MO without SRAFs, the best focus shift range of the high-k absorber mask is smaller than of the reference binary mask, due to the ability of the high-k absorber reduce M3D effects in general.[9,12] However, the best focus shifts of the low-n attPSM are slightly larger with respect to the reference binary mask, due to more pronounced M3D phase effects.[9,11,13]

Below each histogram distribution, the fitting result by Gaussian function is given, where the dark-field mask gives slight larger best focus shifts (mean value of the Gaussian fitting) between the center and edge slits with respect to the bright-field mask, which means that M3D has a slightly larger impact on the dark-field mask at the edge slit.

3.3.2 *Best focus shift of T2Ts*

Figure 11 exhibits the histogram distributions of best focus shifts on T2Ts both for dark-field mask with SRAFs and bright-field mask without SRAFs of these three mask candidates. The high-k absorber mask and the low-n attPSM have very similar best focus shifts of T2Ts with respect to the reference binary mask for both tonalities.

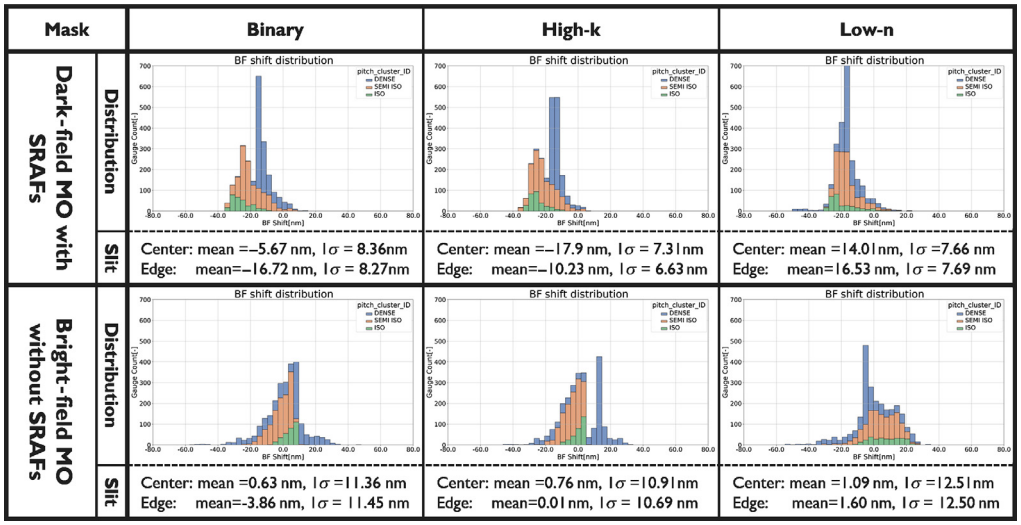

Fig. 10 Histogram distribution of best focus shifts of all the trenches on the design clip. Distribution is fitted by a Gaussian function and the fitting mean and standard deviation (σ) are displayed below each plot.

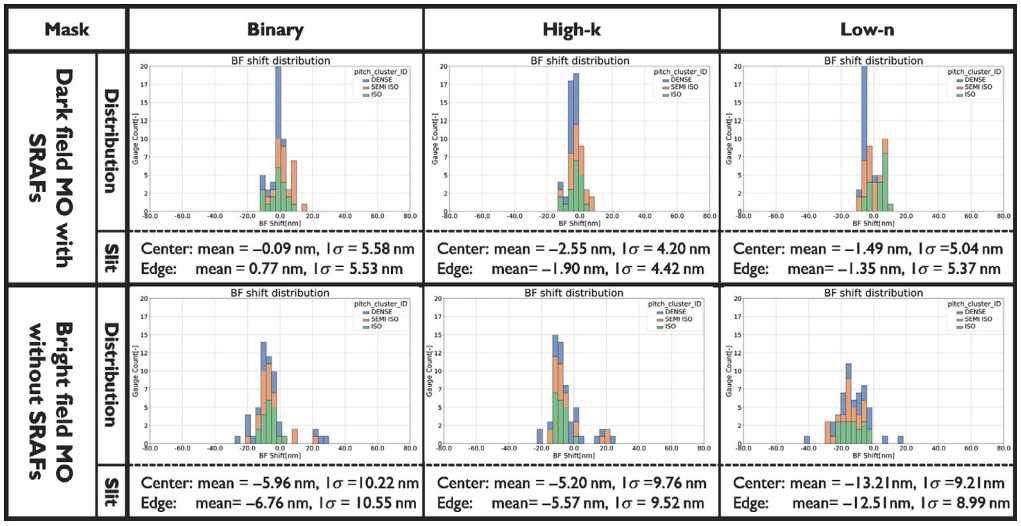

Fig. 11 Histogram distribution of best focus shift of T2Ts for all the T2Ts on the design clip. Distribution is fitted by a Gaussian function and the fitting mean and standard deviation (σ) are displayed below each plot.

3.4 *Impact on MEEF*

3.4.1 *MEEF of trenches*

Figure 12 depicts the MEEF histogram distributions of all the trench features on the design clip at the nominal condition for the center slit. The top row includes the MEEF histogram distributions of dark-field MO with SRAFs, and the bottom row contains the MEEF histogram distributions of bright-field MO without SRAFs. The MEEF distribution of the high-k absorber mask is very similar with respect to the reference binary mask for both tonalities, whereas the low-n attPSM improves the MEEF by ∼20% with respect to the reference binary mask for both mask tonality. Notably, the low-n attPSM has a larger MEEF distribution range than the reference binary mask

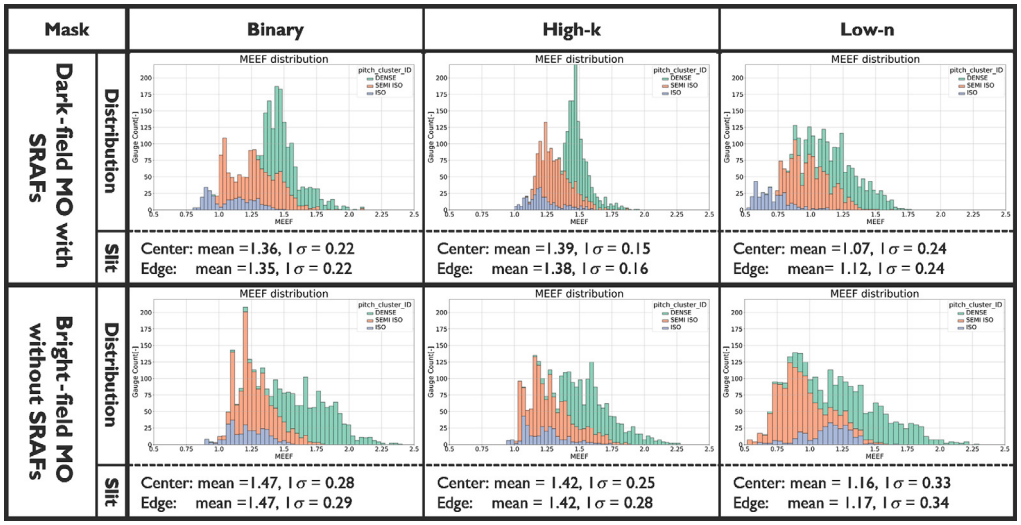

Fig. 12 MEEF histogram distribution of all the trench features on the design clip at nominal condition. Distribution is fitted by a Gaussian function and the fitting mean and standard deviation (σ) are displayed below each plot.

and the high-k absorber mask. Some isolated features and semi-isolated features of the low-n attPSM exhibit a MEEF below one, which means that the low-n attPSM has the ability to reduce the impact of mask errors rather than amplifying them; this implies a larger mask biasing needed for OPC.

3.4.2 *MEEF of T2Ts*

Figure 13 shows the MEEF histogram distributions on T2Ts with respect to these three mask candidates for both dark-field mask with SRAFs and bright-field mask without SRAFs cases at the nominal condition for center slit. All these three mask candidates have very similar MEEF of T2Ts for each tonality. Comparing the tonality per mask absorber, we can see that MEEF of T2Ts is dominated by mask tonality rather than mask type. The T2T MEEF of bright-field mask without SRAFs is much better than of dark-field masks with SRAFs. The similar MEEF distributions are also observed at the edge slit. Moreover, simulations also indicate that bright-field imaging is able to pattern smaller T2T CD.[5]

3.5 *Impact on PPE*

3.5.1 *PPE of trenches*

Figure 14 shows the PPE histogram distribution of all the trench features on the design clip at nominal condition. The table demonstrates that the PPE is dominated by both mask tonality and mask type. Bright-field masks deliver smaller PPE with respect to dark-field masks. The high-k absorber mask has the smallest PPE among these three mask candidates.

3.5.2 *PPE of T2Ts*

Figure 15 shows the PPE histogram distribution of all the T2Ts on the design clip at nominal condition. The dark-field mask of binary and high-k absorber deliver smaller PPE with respect to bright-field mask, whereas low-n attPSM has similar PPE for both tonalities. Comparing Figs. 14 and 15 demonstrate that T2Ts have larger PPE than trenches.

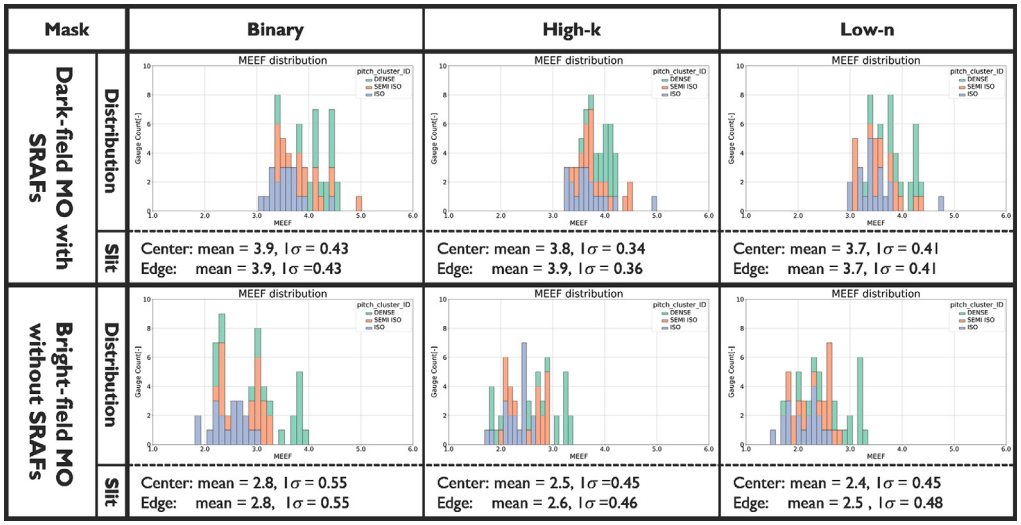

Fig. 13 MEEF histogram distribution on T2Ts of all the T2Ts on the design clip at nominal condition. Distribution is fitted by a Gaussian function and the fitting mean and standard deviation (σ) are displayed below each plot.

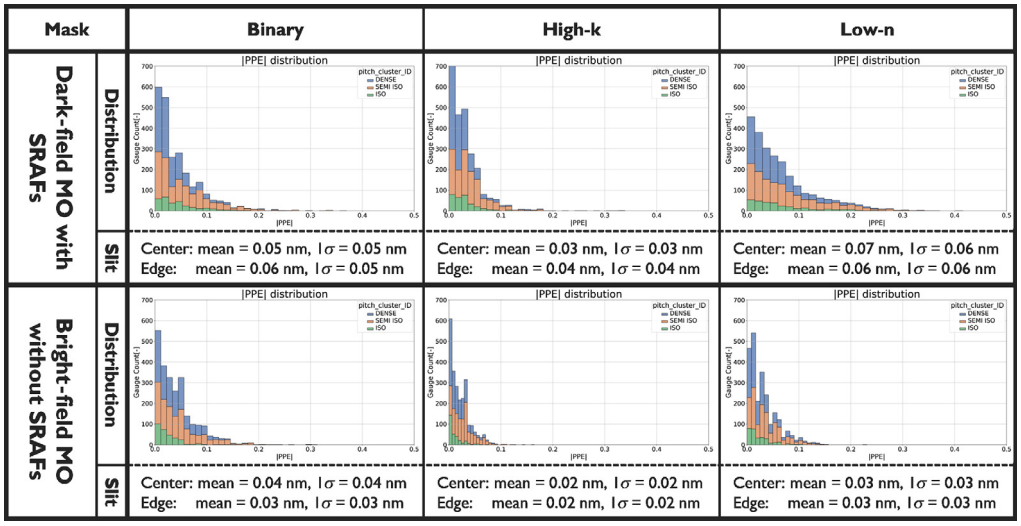

Fig. 14 PPE histogram distribution of all the trench features on the design clip at nominal condition. Distribution is fitted by a Gaussian function and the fitting mean and standard deviation (σ) are displayed below each plot.

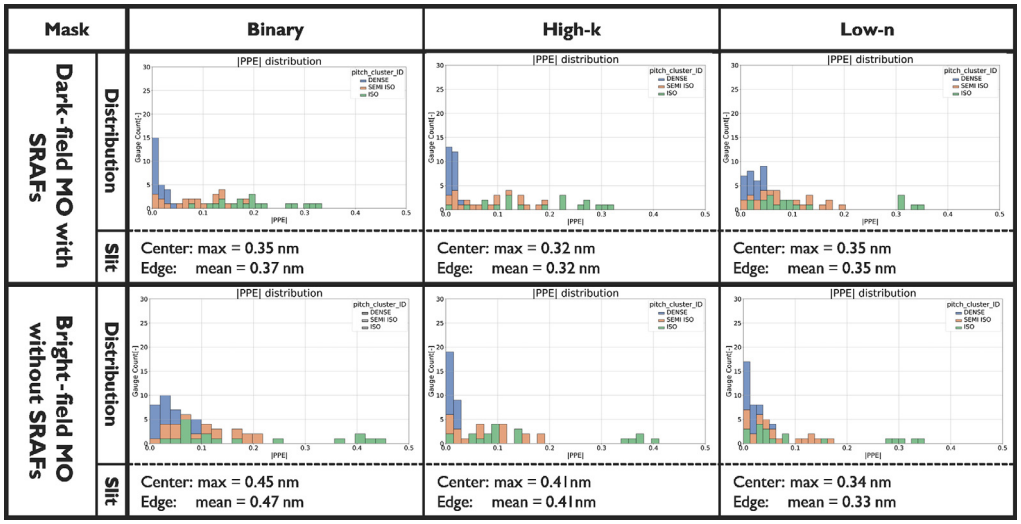

Fig. 15 PPE histogram distribution of all the T2Ts on the design clip at nominal condition. Distribution is fitted by a Gaussian function and the fitting mean and standard deviation (σ) are displayed below each plot.

4 Conclusion

Three mask candidates for 0.33NA EUV single patterning at pitch 28 nm have been explored, using SMO techniques on the M1 layer of an imec N3 random logic design. The impact of both mask tonality and insertion of SRAFs on OPW and pattern fidelity has been evaluated. In general, dark-field masks with SRAFs and bright-field masks without SRAFs deliver the best OPW. Moreover, the impact of alternative mask candidates on the patterning performance of these two options is quantified for various metrics and compared with the reference binary mask: OPW, NILS, best focus shift, MEEF, and PPE. The comparative Fig. 16 summarizes the improvement of each metrics when using these three mask candidates, the best and the worst case for each of the metrics are classified in green and red, respectively.

Mask		Dark-field with SRAFs			Bright-field without SRAFs		
		Binary	High-k	Low-n	Binary	High-k	Low-n
OPW	EL (%)	10	12.5	11.35	11	11.5	13.5
	DoF (nm)	111	114	114	76	83	67
Average NILS	Trenches	2.02	2.05	2.29	2.12	1.93	2.19
	T2Ts	1.16	1.12	1.36	1.33	1.17	1.37
Best focus shift (average/1σ, nm)	Trenches	−5.67/8.36	−17.9/7.31	14.01/7.66	0.63/11.36	0.76/10.91	1.09/12.51
	T2Ts	−0.09/5.58	−2.55/4.2	−1.49/5.04	−5.96/10.22	−5.20/9.76	−13.21/9.21
Average MEEF	Trenches	3.8	3.8	3.7	2.8	2.5	2.5
	T2Ts	1.36	1.39	1.07	1.47	1.42	1.16
PPE (nm)	Trenches	0.05/0.05	0.03/0.03	0.07/0.06	0.04/0.04	0.02/0.02	0.03/0.03
	T2Ts	0.35	0.32	0.35	0.45	0.41	0.35

Fig. 16 Comparative table summarizes the improvement for each of the metrics when using these three mask candidates for patterning imec N3 random logic design, the best and the worst value for each of the metrics are classified in green and red, respectively.

For the dark-field masks with SRAFs, the high-k absorber mask enables better overall EL, smaller best focus shift through pitch and PPE with similar NILS, and MEEF with respect to the reference binary mask; and the low-n attPSM improves the EL, NILS, best focus shift through pitch and MEEF of trenches in overall with slightly larger PPE on trenches. For bright-field masks without SRAFs, the performance of the high-k absorber mask is very similar to the reference binary mask, except for slightly worse NILS of trenches and slightly better PPE. Further absorber thickness optimization is required to obtain the best performance for the high-k absorber mask. The low-n attPSM improves the EL, NILS, MEEF, and PPE, but delivers slightly worse DoF. In general, the bright-field mask enables a significant MEEF improvement on T2Ts with respect to the dark-field mask. Considering all these aspects, simulations indicate that the low-n attPSM performs the best both for dark-field mask with SRAFs and bright-field mask without SRAFs for 0.33NA EUV single patterning at pitch 28 nm.

Currently, imec is taping out a dark-field and a bright-field low-n attPSM. Future investigations will focus on SMO simulation of low-n attPSM using actual mask stack information, mask quality, and MRC values measured from the actual mask. These results will be compared against wafer data obtained from exposing the actual mask on imec's NXE:3400 scanner. Moreover, the optimized source in this paper is only using pitch 28-nm line/space grating as the input target. Adding T2T clips in the SMO to improve the MEEF of T2Ts for the dark-field mask with SRAFs and adding semi-isolated feature clips in the SMO for the bright-field mask without SRAFs to increase the DoF and reduce the best focus shift through pitch will be evaluated and experimentally validated on wafer prints.

Furthermore, high NA (0.55NA) EUVL is required to continue the pitch scaling with EUV single patterning.[33] To prepare for high NA EUVL, the patterning performance of alternative masks will be further assessed using SMO.

Acknowledgments

The authors would like to acknowledge all the contributors from ASML at imec: David Rio, Max Delorme.

References

1. K. Ronse et al., "EUVL is being inserted in manufacturing in 2019: what are the mask related challenges remaining?" *Proc. SPIE* **11177**, 111770A (2019).
2. D. Xu et al., "EUV single patterning exploration for pitch 28 nm," *Proc. SPIE* **11614**, 116140Q (2021).

3. D. Xu et al., "Exploration of alternative mask for 0.33NA EUV single patterning at pitch 28 nm," *Proc. SPIE* **11854**, 118540T (2021).
4. D. Rio et al., "Extending 0.33 NA EUVL to 28 nm pitch using alternative mask and controlled aberrations," *Proc. SPIE* **11609**, 116090T (2021).
5. J.-H. Franke et al., "Metal layer single EUV expose at pitch 28 nm: how bright field and NTD resist advantages align," *Proc. SPIE* **11609**, 116090R (2021).
6. D. D. Simone et al., "28nm pitch single exposure patterning readiness by metal oxide resist on 0.33NA EUV lithography," *Proc. SPIE* **11609**, 116090Q (2021).
7. A. Erdmann et al., "Mask-induced best-focus shifts in deep ultraviolet and extreme ultraviolet lithography," *J. Micro/Nanolithogr. MEMS MOEMS* **15**, 021205 (2016).
8. A. Erdmann et al., "Characterization and mitigation of 3D mask effects in extreme ultraviolet lithography," *Adv. Opt. Technol.* **6**, 187–201 (2017).
9. V. Philipsen et al., "Reducing EUV mask 3D effects by alternative metal absorbers," *Proc. SPIE* **10143**, 1014310 (2017).
10. J.-H. Franke et al., "Improving exposure latitudes and aligning best focus through pitch by curing M3D phase effects with controlled aberrations," *Proc. SPIE* **11147**, 111470E (2019).
11. M. Burkhardt, "Investigation of alternate mask absorbers in EUV lithography," *Proc. SPIE* **10143**, 1014312 (2017).
12. V. Philipsen et al., "Novel EUV mask absorber evaluation in support of next-generation EUV imaging," *Proc. SPIE* **10810**, 108100C (2018).
13. A. Erdmann et al., "Attenuated PSM for EUV: can they mitigate 3D mask effects?" *Proc. SPIE* **10583**, 1058312 (2018).
14. R. Sejpal et al., "Exploring alternative EUV mask absorber for iN5 self-aligned block and contact layers," *Proc. SPIE* **11148**, 111481B (2019).
15. M.-C. van Lare, F. J. Timmermans, and J. Finders, "Alternative reticles for low-k1 EUV imaging," *Proc. SPIE* **11147**, 111470D (2019).
16. J. Finders et al., "Experimental investigation of a high-k reticle absorber system for EUV lithography," *Proc. SPIE* **10957**, 1095714 (2019).
17. A. Erdmann et al., "Perspectives and tradeoffs of absorber materials for high NA EUV lithography," *J. Micro/Nanolithogr. MEMS MOEMS* **19**(4), 041001 (2020).
18. M. Wu et al., "Study of novel EUVL mask absorber candidates," *J. Micro/Nanopattern. Mater. Metrol.* **20**(2), 021002 (2021).
19. V. Philipsen, "Mask is key to unlock full EUVL potential," *Proc. SPIE* **11609**, 1160904 (2021).
20. J. Finders et al., "EUV source optimization driven by fundamental diffraction considerations," *Proc. SPIE* **10450**, 104500C (2017).
21. A. Armeanu et al., "Enabling enhanced EUV lithographic performance using advanced SMO, OPC, and RET," *Proc. SPIE* **10809**, 108090G (2019).
22. M. van de Kerkhof et al., "Enabling sub-10nm node lithography: presenting the NXE:3400B EUV scanner," *Proc. SPIE* **10143**, 101430D (2017).
23. I. A. Makhotkin et al., "Refined extreme ultraviolet mask stack model," *J. Opt. Soc. Am. A* **38**, 498–503 (2021).
24. S. Hsu et al., "An innovative source-mask co-optimization (SMO) method for extending low k1 imaging," *Proc. SPIE* **7140**, 714010 (2008).
25. D. Zhang et al., "Source mask optimization methodology (SMO) and application to real full chip optical proximity correction," *Proc. SPIE* **8326**, 83261V (2012).
26. D. Rio et al., "EUV pupil optimization for 32 nm pitch logic structures," *Proc. SPIE* **10809**, 108090N (2018).
27. H. J. Levinson and T. A. Brunner, "Current challenges and opportunities for EUV lithography," *Proc. SPIE* **10809**, 1080903 (2018).
28. L. Meli et al., "Defect detection strategies and process partitioning for SE EUV patterning," *Proc. SPIE* **10583**, 105830E (2018).
29. P. D. Bisschop and E. Hendrickx, "Stochastic printing failures in EUV lithography," *Proc. SPIE* **10957**, 109570E (2019).
30. S. G. Hansen, "Photoresist and stochastic modeling," *J. Micro/Nanolithogr. MEMS MOEMS* **17**(1), 013506 (2018).

31. M.-C. van Lare et al., "Optimizations aspects for EUV low-k1 logic with the low-n mask," *Proc. SPIE* **11854**, 1185412 (2021).
32. I. Mochi et al., "Assist features: placement, impact, and relevance for EUV imaging," *Proc. SPIE* **9776**, 97761S (2016).
33. J. van Schoot et al., "High-NA EUV lithography exposure tool progress," *Proc. SPIE* **10957**, 1095707 (2019).

Dongbo Xu is presently a R&D engineer at imec. He received his PhD in the field of computational lithography from Friedrich-Alexander-University Erlangen-Nürnberg in 2016 and his ME degree from the University of Chinese Academy of Sciences. His fields of interest include optical and EUV lithography simulation, OPC modeling, and image processing with machine learning

Biographies of the other authors are not available.